Supporting Information

In-MOF-derived In_2S_3/Bi_2S_3 heterojunction for enhanced photocatalytic hydrogen production

Sibi Liu[1,2], Yijin Wang[1,2], Youzi Zhang[1,2], Xu Xin[1,2], Peng Guo[1,2], Dongshan Deng[1,2], Jahan B. Ghasemi[3], Miao Wang[1,2], Ruiling Wang[1,2*], Xuanhua Li[1,2*]

[1]Shenzhen Research Institute of Northwestern Polytechnical University, Shenzhen 518057, China

[2]State Key Laboratory of Solidification Processing, Center for Nano Energy Materials, School of Materials Science and Engineering, Northwestern Polytechnical University, Xi'an 710072, China

[3]Department of Chemistry, University of Tehran, District 6, Tehran (Iran)

*Corresponding author E-mail: lixh32@nwpu.edu.cn; wangruiling@nwpu.edu.cn

Methods

Materials. The indium nitrate hydrate ($In(NO)_3 \cdot 4H_2O$, ≥ 99.99 %), *p*-phthalic acid (PTA, ≥ 99 %), bismuth nitrate pentahydrate ($Bi(NO)_3 \cdot 5H_2O$, ≥ 99 %), polyvinylpyrrolidone (PVP, average molecular weight 58000), ethylene glycol ($C_2H_6O_2$, ≥ 98 %), N,N-dimethylformamide (DMF, ≥ 99.9 %), thiourea (CH_4N_2S, ≥ 99 %) and sodium sulfite anhydrous (Na_2SO_3, ≥ 98 %) were purchased from Sigma-Aldrich and used without further purification.

Synthesis of In-MOF. The In-MOF was synthesized using the previous reported method by Moonhyun Oh [1]. 0.11 g of $In(NO)_3 \cdot 4H_2O$ and 0.108 g of PTA were added to 30 mL of DMF followed by stirring for 30 min. After that, the solution was heated at 100 ℃ for 6 h. After natural cooling, the product was cleaned with ethanol three times. Finally, the white powder was obtained by vacuum drying at 60 ℃ for 12 h.

Synthesis of In_2S_3. The as-prepared In-MOF was vulcanized in a chemical vapor deposition furnace to produce the In_2S_3. Specifically, the In-MOF was placed in a relatively higher temperature region of the furnace, while the sulfur powder was placed in a lower temperature region, and the air was removed by argon gas passing through the furnace at a flow rate of 100 cm^3/min for 30 min. The low and high temperature regions were then heated from room temperature to 250 ℃ (5 ℃/min) and 500 ℃ (10 ℃/min), respectively. The heat-treatment process was maintained for 30 min before the system was cooled to room temperature at an argon atmosphere.

Synthesis of In_2S_3/Bi_2S_3. The obtained In_2S_3 was dispersed into 35 mL of ethylene glycol mixed solution, which contained 0.01 g of PVP, 0.01 g of thiourea, and 0.01 g of $Bi(NO)_3 \cdot 5H_2O$. After 30 min of ultrasonic dispersion, the uniform solution was transferred into a 50 mL Teflon-lined stainless-steel autoclave and heated at 140 °C for 8 h. After cooling down, the product was cleaned by ethanol and water three times, respectively. The In_2S_3/Bi_2S_3 powder was obtained after drying under vacuum

condition. As a comparison, the flower-like Bi_2S_3 was synthesized using the same process without In_2S_3 addition.

Characterization of the photocatalysts. The X-ray diffractometer (labX XRD-7000) with Cu Kα1 (λ = 0.1541 nm) radiation was performed to analyze the crystalline structure and phase composition of the samples. The morphology of photocatalysts was observed by using scanning electron microscopy (SEM, FEI Nova) and transmission electron microscopy (TEM, FEI Tecnai F30G2). A Raman spectrometer (Renishaw InVia) was used to acquire the Raman spectra of photocatalysts using a laser excitation of 532 nm. The ultraviolet-visible (UV-Vis) spectra of the samples were examined using a UV-Vis spectrophotometer (Perkin-Elmer Lambda 35 UV-VIS-NIR). A photoluminescence spectrometer (FLS 980) was used to observe the steady-state photoluminescence (PL) spectra of the samples at a 325 nm wavelength. The chemical combination and electronic state between the elements were obtained by X-ray photoelectron spectroscopy (XPS, AXIS Supra). Ultraviolet photoelectron spectroscopy (UPS) was performed in an XPS with an excitation source of He I (21.22 eV). The power density was measured using the optical power meter (CEL-NP2000-2). The Brunauer-Emmett-Teller (BET) surface areas of samples were measured in Micromeritics ASAP2010 equipment.

Photocatalytic hydrogen production reaction. For photocatalytic performance evaluation, 50 mg of the photocatalyst was dissolved in 50 mL of 0.5 M Na_2SO_3 aqueous solution and stirred for 10 min. The photocatalytic hydrogen production reaction was conducted in a vacuum reactor with a 100 mW/cm^2 Xe lamp serving as the light source. The temperature was kept at 5 ℃ by a recirculating cooling water system during the light irradiation. The evolved gas was extracted into the gas chromatography (Shimadzu GC-2014c) equipped with a thermal conductivity detector with argon used as the carrier gas throughout the reaction process.

Photoelectrochemical measurements. All photoelectrochemical measurements were conducted on an electrochemical workstation (Chenhua 760) with a three-electrode system. The Pt electrode,

Ag/AgCl electrode, and fluorine-doped tin oxide (FTO) glass covered with photocatalyst (an active area of 1.5 × 0.75 cm^2) were used as a counter electrode, reference electrode, and working electrode, respectively. Besides, the 0.5 M Na_2SO_3 solution was used as the electrolyte in order to ensure the consistency of the photocatalytic process. The working electrode was prepared by dispersing 8 mg of photocatalyst in a mixed solution which contains 495 μL of ethanol, 495 μL of water, and 10 μL of Nafion. Then, an ultrasound was used to mix the solution evenly for 10 min. The 100 μL of mixture was coated onto the FTO glass electrode. Electrochemical impedance spectroscopy (EIS) was performed in the frequency range of 10^{-2} to 10^5 Hz with a bias voltage of 0.3 eV (versus Ag/AgCl). The Mott-Schottky (M-S) curves were tested at a frequency of 1000 Hz in the dark. The photocurrent response performance was tested at 0 eV (versus Ag/AgCl) under the irradiation of a 100 mW/cm^2 Xe arc lamp.

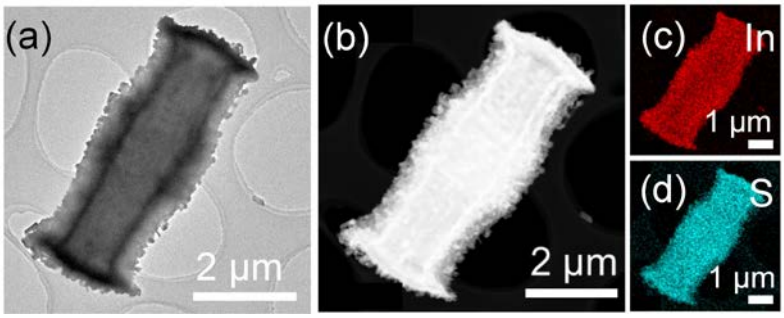

Fig. S1 Micromorphology of In_2S_3.

(a) TEM image; (b−d) EDX elemental mapping images of In, S elements for In_2S_3.

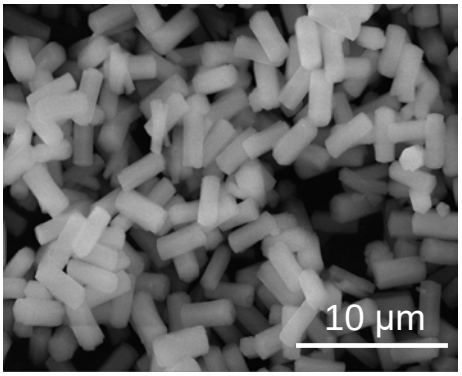

Fig. S2 SEM image of In-MOF precursor.

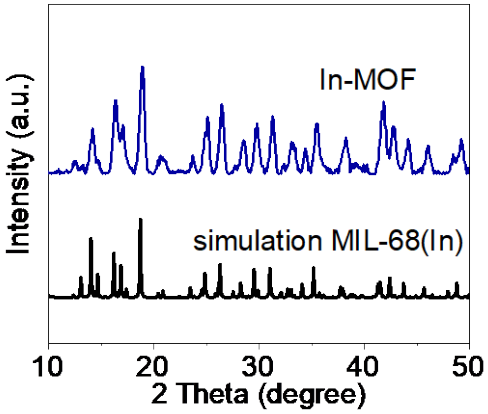

Fig. S3 XRD pattern of In-MOF precursor.

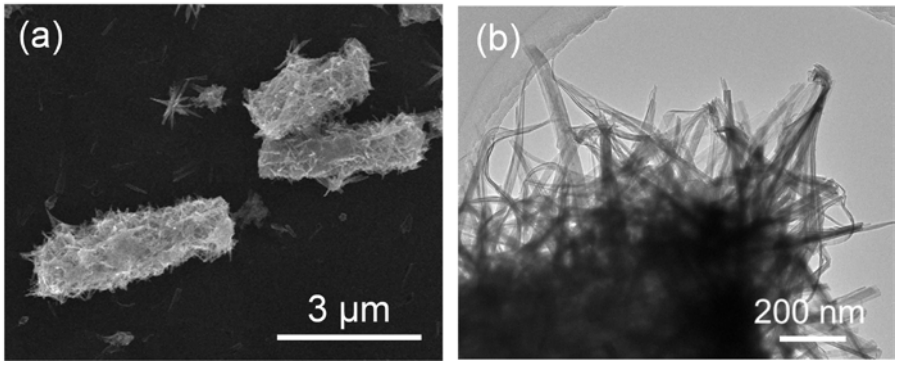

Fig. S4 Micromorphology of In_2S_3/Bi_2S_3 after catalytic reaction.

(a) SEM; (b) TEM images of In_2S_3/Bi_2S_3 after 20 h photocatalytic test.

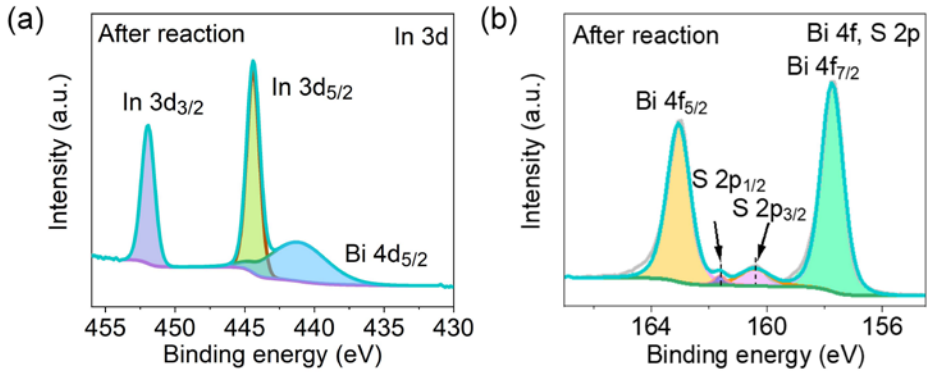

Fig. S5 Chemical structure of In_2S_3/Bi_2S_3 after catalytic reaction.

(a) XPS spectrum of In 3d for In_2S_3/Bi_2S_3 after 20 h photocatalytic test; (b) XPS spectra of Bi 4f and S 2p of In_2S_3/Bi_2S_3 after 20 h photocatalytic test.

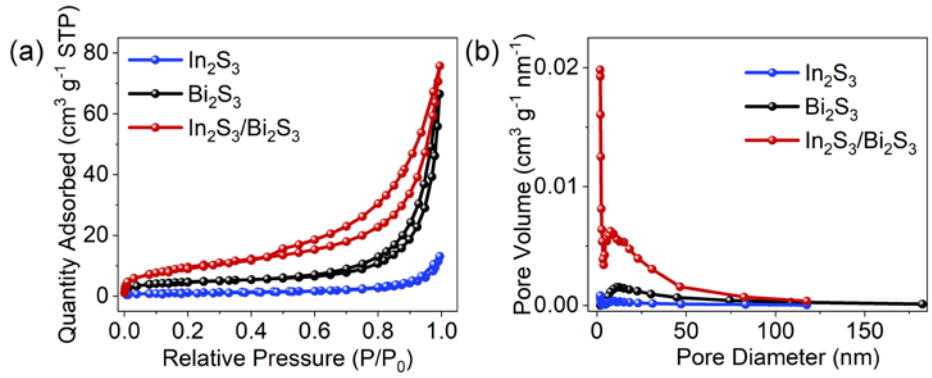

Fig. S6 Specific surface areas characterization of In_2S_3/Bi_2S_3.

(a) N_2 adsorption-desorption isotherms; (b) pore size distribution curves of In_2S_3, Bi_2S_3 and In_2S_3/Bi_2S_3.

The N_2 adsorption-desorption measurements show that all of the samples exhibit type IV isotherm. The Brunauer-Emmett-Teller (BET) surface area of the In_2S_3/Bi_2S_3 heterojunction is 30.0325 m^2/g, which is much larger than that of In_2S_3 (6.1001 m^2/g) and Bi_2S_3 (16.3591 m^2/g). The pore size distribution analyses of samples show that the pore size distributions of all samples range from 2 to 50 nm. The high surface area of the In_2S_3/Bi_2S_3 heterojunction provides abundant adsorption sites for surface reaction, which benefits for the photocatalytic hydrogen evolution activity.

Table S1 Summary of photocatalytic hydrogen production performance for analogous heterojunctions.

Catalysts	Light source	Sacrificial agent	H_2 production rate/(mmol·(g· h)$^{-1}$)	Ref.
In_2S_3/Bi_2S_3	λ > 300 nm	Na_2SO_3	0.71	This paper
$MoS_2@In_2S_3/Bi_2S_3$	λ > 420 nm	methanol	0.97	[2]
CdS/Bi_2S_{3-Vs}	300 W Xe arc lamp	Na_2S/Na_2SO_3	0.54	[3]
Yb-Bi_2S_3 QDs/TiO_2	λ > 420 nm	TEOA	0.079	[4]
ZnO multipod Ag@Bi_2S_3	250 W high pressure Hg lamp	Na_2S/Na_2SO_3	0.22	[5]
Ag/Bi_2S_3/MoS_2	λ > 420 nm	methanol	0.53	[6]
In_2S_3/Mo_2C	λ > 420 nm	lactic acid	0.54	[7]
$In_2S_3/Nb_2O_5/Nb_2C$	λ > 420 nm	TEOA	0.69	[8]
In_2S_3/g-C_3N_4	420−780 nm	–	0.31	[9]
In_2S_3/In_2O_3	300 W Xe arc lamp	TEOA	0.137	[10]

References

[1] Cho W, Lee H J, Oh M. Growth-controlled formation of porous coordination polymer particles. Journal of the American Chemical Society, 2008, 130(50): 16943−16946

[2] Wang Y, Xing Z, Zhao H, et al. MoS_2@In_2S_3/Bi_2S_3 core-shell dual Z-scheme tandem heterojunctions with broad-spectrum response and enhanced photothermal-photocatalytic performance. Chemical Engineering Journal, 2022, 431: 133355−133365

[3] Li M, Yao H, Yao S, et al. Vacancy-induced tensile strain of CdS/Bi_2S_3 as a highly performance and robust photocatalyst for hydrogen evolution. Journal of Colloid and Interface Science, 2023, 630: 224−234

[4] Miodyńska M, Mikolajczyk A, Bajorowicz B, et al. Urchin-like TiO_2 structures decorated with Lanthanide-doped Bi_2S_3 quantum dots to boost hydrogen photogeneration performance. Applied Catalysis B: Environmental, 2020, 272: 118962−118978

[5] Mandal S, Ananthakrishnan R. Double effects of interfacial Ag nanoparticles in a ZnO multipod@Ag@Bi_2S_3 Z-scheme photocatalytic redox system: concurrent tuning and improving charge-transfer efficiency. Inorganic Chemistry, 2020, 59(11): 7681−7699

[6] Jiang H, Xing Z, Zhao T, et al. Plasmon Ag nanoparticle/Bi_2S_3 ultrathin nanobelt/oxygen-doped flower-like MoS_2 nanosphere ternary heterojunctions for promoting charge separation and enhancing solar-driven photothermal and photocatalytic performances. Applied Catalysis B: Environmental, 2020, 274: 118947−118956

[7] Ma X, Ren C, Li H, et al. A novel noble-metal-free Mo_2C-In_2S_3 heterojunction photocatalyst with efficient charge separation for enhanced photocatalytic H_2 evolution under visible light. Journal of Colloid and Interface Science, 2021, 582: 488−495

[8] Tayyab M, Liu Y, Liu Z, et al. One-pot in-situ hydrothermal synthesis of ternary In_2S_3/Nb_2O_5/Nb_2C Schottky/S-scheme integrated heterojunction for efficient photocatalytic hydrogen production. Journal of Colloid and Interface Science, 2022, 628: 500−512

[9] Guo B, Liu B, Zhang X, et al. In_2S_3 nanosheets growing on sheet-like g-C_3N_4 as high-performance photocatalyst for H_2 evolution under visible light. International Journal of Energy Research, 2022, 46(7): 9138−9149

[10] Liu M, Li P, Wang S, et al. Hierarchically porous hydrangea-like In_2S_3/In_2O_3 heterostructures for enhanced photocatalytic hydrogen evolution. Journal of Colloid and Interface Science, 2021, 587: 876−882